Fuel 384 (2025) 133950

Contents lists available at ScienceDirect

Fuel

journal homepage: www.elsevier.com/locate/fuel

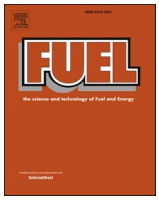

Full Length Article

Fate of phosphorus and potassium in gasification of wheat bran and sunflower seed shells

Daniel Schmid [a,*], Emil Lidman Olsson [b], Emil Vainio [a], Hao Wu [b], Oskar Karlström [c], Leena Hupa [a]

[a] High-Temperature Processes and Materials, Åbo Akademi University, Henrikinkatu 2, 20500 Turku, Finland
[b] CHEC Research Centre, Department of Chemical and Biochemical Engineering, Technical University of Denmark, Søltofts Plads, Building 229, 2800 Kgs Lyngby, Denmark
[c] Industrial Engineering and Management, Department of Mechanical and Materials Engineering, University of Turku, 20014 Turku, Finland

ARTICLE INFO

Keywords:
Biomass
Waste
Valorization
Phosphorus
Gasification

ABSTRACT

Thermal conversion of agricultural biomass residues poses a great opportunity to valorize waste materials by recovering energy and valuable elements such as phosphorus. Utilizing biomass residues in thermal conversion is, on the other hand, often coupled with operational challenges due to particle emissions, deposit formation, corrosion and slagging caused by the ash-forming elements in the biomass. A detailed understanding of the ash chemistry is required when utilizing those fuels to reduce these operational problems and recover valuable elements from the ash. However, predictions for ash transformation are often always reliable when using existing thermodynamic data and ash transformation mechanisms. The present work investigated the release of phosphorus and potassium during gasification of two seed-originated agricultural biomass residues, wheat bran and sunflower seed shells, at 900–1100 °C in 3 % O_2 or 10 % CO_2 (rest N_2). The residues were characterized by scanning electron microscopy (SEM), X-ray diffraction (XRD) and inductively coupled plasma optical emission spectroscopy (ICP-OES). During the gasification of wheat bran, phosphorus and potassium were partly released to the gas phase, while only potassium was released to the gas phase during the gasification of sunflower seed shells. The residues from the gasification of wheat bran contained mainly K-Mg-phosphates, while phosphorus was identified as hydroxyapatite in the sunflower seed shell residues. The experimental observations for wheat bran are in contradiction with predictions from thermodynamic equilibrium calculations, which suggest that all phosphorus remains in the residues. The discrepancy between the experimental and calculated results may be due to carbothermic reduction of phosphates, i.e. reactions between phosphates and carbon. As the occurrence of carbothermic reduction reactions is connected to the kinetics of the carbon consumption, it is suggested that thermodynamic data alone is not sufficient to correctly predict the ash chemistry in thermal conversion processes of phosphorus rich biomass fuels.

1. Introduction

Agricultural biomass waste has increasingly gained interest as an energy source due to the increasing demand for alternative fuels to replace fossil fuels in heat and power generation and industrial processes. Agricultural biomass waste, however, has many disadvantages in direct utilization as a fuel such as low heating values compared to coal and high ash contents, which may cause operational problems. One method that may be applied to make these fuels more accessible for a wider usage is gasification [1]. Gasification is a complex process, in which a solid fuel is converted thermochemically into syngas, which, after purification, can be used for further processing [2]. The remaining char consists mainly of unreacted carbon and ash. Ash-forming elements may cause operational problems such as bed agglomeration [3,4], deposit formation and subsequent corrosion of heat exchange surfaces [5,6], or contamination of the syngas, depending on if they remain in the residue or are evaporated during the gasification process [7,8]. Additionally, those elements may also interfere with exhaust gas cleaning systems which rely on catalysts [9,10]. Hence, it is important to understand the release mechanism and chemistry of ash forming elements

* Corresponding author.
E-mail address: dschmid@abo.fi (D. Schmid).

https://doi.org/10.1016/j.fuel.2024.133950
Received 22 July 2024; Received in revised form 2 October 2024; Accepted 27 November 2024
Available online 2 December 2024

Table 1
Elemental analysis of wheat bran (WB) and sunflower seed shells (SSS) in mg/kg.

	WB	SSS
wt.-% ds		
C	42.8 ± 0.1	47.4 ± 0.7
H	6.54 ± 0.09	5.81 ± 0.08
N	2.58 ± 0.07	0.69 ± 0.02
S	0.07 ± 0.01	< 0.01
mg/kg ds		
Al	586 ± 3	659 ± 19
Ca	675 ± 6	3440 ± 2
Fe	167 ± 1	122 ± 1
K	9158 ± 183	8164 ± 111
Mg	2588 ± 6	1641 ± 7
Mn	149 ± 1	283 ± 2
P	9682 ± 390	1643 ± 55
Si	578 ± 5	2450 ± 21
Cl	552 ± 11	1260 ± 17

to reduce operational problems and optimize gasification processes. Two challenging elements in this context are phosphorus [11,12] and potassium [13,14].

Phosphorus and potassium are crucial elements not only when operational issues in thermal conversion processes of agricultural biomass fuels are considered. Both elements also play an important role when considering the possible utilization of biomass ashes, e.g. for usage in fertilizers [15,16]. Phosphorus and potassium are vital nutrients for plants and animals with increasing demands. Phosphorus production costs are continuously increasing as phosphate ores less abundant in phosphorus need to be exploited to meet the demand [17]. Agricultural biomass ashes are often rich in phosphorus and potassium and provide a potential for valorization of the ash and recovery of these elements [18,19]. Especially seed-originated biomasses contain high amounts of phosphorus and potassium [20,21]. To be able to utilize ashes, characterization of the ash is necessary. Characterization of biomass ashes is challenging due to the great variety of chemical compositions and properties depending on the fuels and the conditions of the thermal conversion process [18,22]. It is possible to predict the properties of biomasses, both related to operational problems and for the use of ash, with thermodynamic equilibrium calculations, but these predictions are unreliable for many phosphorus-containing biomasses [23]. Earlier studies showed the discrepancy between thermodynamic equilibrium calculations and experimental results, showing the necessity to improve and expand thermodynamic data and the understanding of reaction mechanisms to improve predictions [12,24].

The present study investigated the release of ash forming elements, with a specific focus on phosphorus and potassium during gasification of seed-originated biomass fuels. Residues from gasification of wheat bran and sunflower seed shells were characterized with SEM and XRD, and the release of phosphorus and potassium to the gas phase during the experiment was determined based on the elemental analysis. The gasification experiments were conducted under well-controlled conditions at 900 – 1100 °C, a temperature range relevant for fluidized bed gasification. Another focus of this study is the evaluation of how well thermodynamic equilibrium calculations can predict ash transformation based on existing data. Thermodynamic equilibrium calculations were performed for such conditions that were investigated in the experiments and the data was compared with the experimental results. Both the experimental and calculated data is important to improve our knowledge about ash transformation and release mechanisms during thermal conversion processes.

2. Materials and methods

2.1. Fuels

Two agricultural biomass fuels were investigated: wheat bran (WB) and sunflower seed shells (SSS). The fuels were used as pellets with 6 mm (WB) or 8 mm (SSS) diameter and 1–2 cm length. These fuels were selected as they differ significantly in their chemical composition. Wheat bran is rich in phosphorus and potassium and contains significant amounts of magnesium. Sunflower seed shells also contain much potassium, but less phosphorus and are rich in calcium and silica. The concentrations of the main ash-forming elements are given in Table 1. For the determination of the ash forming elements, fuel samples were first dissolved in a mixture of HNO_3 (65 %), H_2O_2 (30 %) and HBF_4 (50 %) with a volume ratio of 5:1:1 following analysis (5 repetitions) using an inductively coupled plasma optical emission spectrometer of the type Optima 5300 DV.

2.2. Pyrolysis and gasification

Fig. 1 shows the experimental setup used for the thermal conversion experiments. A detailed description of the setup can be found elsewhere [20]. Fuel samples were placed into the inner tube in an Al_2O_3 crucible. The inner tube was flushed with the primary gas to create the desired conditions for the experiment. A secondary gas stream could be added to oxidize reaction products coming from the inner tube into the outer tube when necessary.

In the first stage, the fuel samples were pyrolyzed in pure N_2 (3 Nl/min) at 800 °C to produce a char. Approximately 10 g of biomass sample was pyrolyzed at a time and kept for 5 min in the reactor. The char was then used for the gasification experiments. This was done to ensure to have enough sample mass after the gasification experiments to get reliable analysis of the residues remaining after the gasification experiments. Gasification was done using 2.5 g of biomass char from WB or SSS in 3 % O_2 at 1000 °C. The samples were kept in the reactor for 3 h and then slowly cooled down to room temperature. Char samples from

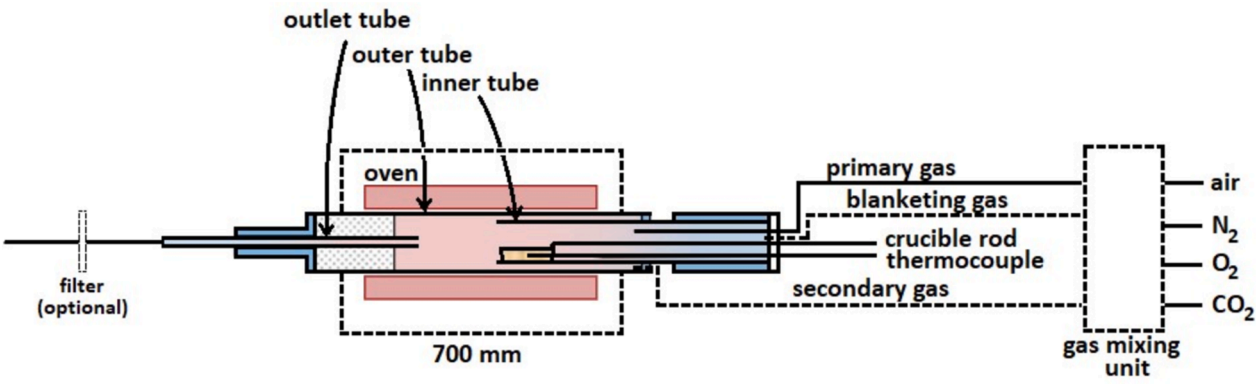

Fig. 1. Schematic drawing of the horizontal tube reactor [20].

Table 2
Databases used for the thermodynamic equilibrium calculations.

Database	Full name solution
FactPS	*Pure gas phases*: KOH, NO, NO_2, HONO, OH, HOO, HOOH, PO, PO_2, $(P_2O_3)_2$, $(P_2O_5)_2$ *Pure solid phases:* $KHPO_4$, K_2HPO_4, $CaHPO_4$, $Mg_2SiO_4(s_3)$, $Mg_3Si_2O_5(OH)_4$, $Mg_3Si_4O_{10}(OH)_2$, $Mg_7Si_8O_{22}(OH)_2$, $(CaO)(SiO_2)_2(H_2O)_2$, $(CaO)_3(SiO_2)_2(H_2O)_3$, $(CaO)_4(SiO_2)_6(H_2O)_5$, $(CaO)_5(SiO_2)_6(H_2O)_3$, $(CaO)_6(SiO_2)_6(H_2O)$, $(CaO)_8(SiO_2)_6(H_2O)_3$, $(CaO)_{10}(SiO_2)_{12}(H_2O)_{11}$, $(CaO)_{10}(SiO_2)_{12}(H_2O)_{21}$, $(CaO)_{12}(SiO_2)_6(H_2O)_7$, $Ca_2Mg_5Si_8O_{22}(OH)_2$, $CaHPO_4$, $CaHPO_4(H_2O)_2$, $Ca(H_2PO_4)_2(H_2O)$, $Ca_5HO_{13}P_3$
FToxide	*Pure solid phases*: MgO, SiO_2, $MgSiO_3$, Mg_2SiO_4, P_2O_5, MgP_2O_6, $Mg_2P_2O_7$, $Mg_3P_2O_8$, MgP_4O_{11}, P_2SiO_7, $P_4Si_3O_{16}$, K_2O, K_6MgO_4, K_2SiO_3, $K_2Si_2O_5$, $K_2Si_4O_9$, K_4SiO_4, K_2MgSiO_4. $K_2MgSi_3O_8$, $K_2MgSi_5O_{12}$. $K_2Mg_5Si_{12}O_{30}$, $K_4Mg_2Si_5O_{14}$, $K_{10}Mg_5Si_{11}O_{32}$, KPO_3, K_3PO_4, $K_4P_2O_7$, $K_5P_3O_{10}$, CaO, $CaSiO_3$, Ca_2SiO_4, Ca_3SiO_5, $Ca_3Si_2O_7$, $CaMgSi_2O_6$, $Ca_2MgSi_2O_7$, $Ca_3MgSi_2O_8$, CaP_2O_6, CaP_4O_{11}, $Ca_2P_2O_7$, $Ca_2P_6O_{17}$, $Ca_3P_2O_8$, $Ca_4P_2O_9$, $Ca_4P_6O_{19}$, $Ca_3Mg_3(PO_4)_4$, $Ca_4Mg_2P_6O_{21}$, $Ca_5P_2SiO_{12}$, $Ca_7P_2Si_2O_{16}$, K_2CaSiO_4, $K_4CaSi_3O_9$, $K_4CaSi_6O_{15}$, $K_8CaSi_{10}O_{25}$, $K_2Ca_2Si_2O_7$, $K_2Ca_2Si_9O_{21}$, $K_2Ca_3Si_6O_{16}$, $K_2Ca_6Si_4O_{15}$
FTsalt	*Pure solid phases:* MgO, $Mg(OH)_2$, K_2O, KOH, CaO, $Ca(OH)_2$
GTOX	*Pure gas phase*: N_2, O_2, H_2O, CO, CO_2, Cl_2, HCl, K, KCl, P, P_2, P_3, P_4, P_2O_5 *Pure solid phases*: MgO, SiO_2, $MgSiO_3$, Mg_2SiO_4, MgP_2O_6, MgP_2O_7, $Mg_3(PO_4)_2$, $K_2Si_2O_3$, $K_2Si_2O_5$, $K_2Si_4O_9$, K_2MgSiO_4, $K_2MgSi_3O_8$, $K_2Mg_5Si_{12}O_{30}$, $K_4Mg_2Si_5O_{14}$, $K_{10}Mg_5Si_{11}O_{32}$, KPO_3, K_3PO_4, $K_4P_2O_7$, $KPMgO_4$, $KMgP_3O_9$, $KMg_4P_3O_{12}$, $K_2MgP_2O_7$, $K_2P_4MgO_{12}$, $K_4P_2MgO_8$, $K_4P_6Mg_4O_{21}$, $K_6MgP_2O_9$, $CaSiO_3$, Ca_2SiO_4, Ca_3SiO_5, $Ca_3Si_2O_7$, $CaMgSiO_4$, $CaMgSi_2O_6$, $Ca_2MgSi_2O_7$, $Ca_3MgSi_2O_8$, CaP_2O_6, CaP_4O_{11}, $Ca_2P_2O_7$, $Ca_2P_6O_{17}$, $Ca_3P_2O_8$, $Ca_4P_2O_9$, CaP_2MgO_7, $Ca_3P_4Mg_3O_{16}$, $Ca_5P_2SiO_{12}$, $Ca_7P_2Si_2O_{16}$, $Ca_2P_2SiMg_3O_{12}$, CaK_2SiO_4, $CaK_4Si_3O_9$, $CaK_4Si_6O_{15}$, $CaK_8Si_{10}O_{25}$, $Ca_2K_2Si_9O_{21}$, $Ca_3K_2Si_6O_{16}$, $CaKPO_4$, $CaKP_3O_9$, $CaK_2P_2O_7$, $CaK_4P_2O_8$, $CaK_6P_2O_9$ *GTOX-SLIQ*: $K_4Si_2O_6$, $K_2Si_2O_5$, $K_2Si_4O_9$, $CaSiO_3$, Ca_2SiO_4, $MgSiO_3$, Mg_2SiO_4, CaK_2SiO_4, K_2MgSiO_4, $K_2MgSi_5O_{12}$, CaP_2O_6, $Ca_2P_2O_7$, $Ca_3(PO_4)_2$, $Mg_2P_2O_7$, $Mg_3(PO_4)_2$, MgP_2O_6, KPO_3, K_3PO_4, $K_4P_2O_7$, $KCaP_3O_9$, $KMgPO_4$, K_2CO_3, $CaCO_3$, $MgCO_3$ *MeO*: CaO, MgO *GTOX-K3PH*: $(K_2O)_2(P_2O_5)(K_2O)$,$(K_2O)_2(P_2O_5)(CaO)$, $(K_2O)_2(P_2O_5)(K_2CaO_2)$, $(K_2O)_2(P_2O_5)(MgO)$, $(K_2O)_2(P_2O_5)(K_2MgO_2)$ GTOX-MeO: CaO, MgO

SSS were also gasified in 3 % O_2 at 900 or 1100 °C and in 10 % CO_2 at 900, 1000 and 1100 °C. Additional tests were performed with char from WB, in which a filter was added to the outlet tube of the reactor to condense and absorb species released to the gas phase during the gasification at room temperature. The residuals from the gasification experiments were analyzed using SEM-EDS, ICP-OES, and XRD. For the SEM-analysis, sample particles were dispersed on double-sided carbon tape mounted on aluminum stubs. Images of the residues were obtained using a Prisma E scanning electron microscope from Thermo Scientific at 20 kV using the secondary electron signal. The elemental distribution was obtained with EDS at 20 kV using the backscattered electron signal. The ICP-OES analysis of the residues was performed in the same way as for the fuel samples described previously. The powder diffraction patterns from the XRD analysis were collected using a Huber G670 powder diffractometer. Samples were analyzed in the 2θ range 3.5 to 100°, with a step size of 0.005°, using CuKα1 radiation (λ = 1.54056 Å) for 1 h. The data were collected in transmission mode from a rotating flat plate inclined 45° relative to the primary beam. The software Crystallographica Search-Match, version 3.1.0.2, with ICDD's (International Centre for Diffraction Data) PDF-4 + 2022 database, was used for the evaluation.

2.3. Thermodynamic equilibrium calculations

Thermodynamic equilibrium calculations were performed to predict which stable phases will form in the residue under gasification conditions. Those predictions were used for comparison with the experimental results from SEM-EDS and XRD analysis. The Equilib tool from the Software *FactSage 8.3* [25] was used for the equilibrium calculations using the databases *FactPS*, *FToxid*, *FTsalt* and GTOX. The phases used for the calculations are listed in Table 2. The input data for the calculations was based on the elemental analysis of the biomasses (ash-forming elements and carbon, hydrogen and oxygen from the fuel). N_2, O_2, CO_2 were added to get a reasonable simulation of the gasification conditions used in the experiments. For the calculations, 10 g of the fuel + 20 mol of gas mixture was used. This ratio of fuel to gas mixture was chosen to provide excess oxygen for the complete conversion of the char, to mimic the conditions of the experiments in which a continuous flow was added to the reactor until the char was fully converted. The results are sensitive to the fuel and gas mixture ratio, mainly due to the amount of oxygen available for reaction.

3. Results and discussion

3.1. Wheat bran

The char yield of wheat bran after pyrolysis in N_2 at 800 °C was 22.5 ± 0.3 %. In the subsequent gasification experiment in 3 % O_2 at 1000 °C, 2.5 g of char was used, forming a 610 mg residue after 3 h in the reactor. A SEM image and EDS analysis of the residues are presented in Fig. 2. The SEM image reveals large homogenous particles which may be explained by melting during the experiment. The EDS analysis confirms the samples homogeneity, exhibiting an even distribution of potassium, phosphorus and magnesium in the particles. Potassium and magnesium phosphates, along with calcium and aluminum phosphates, were identified through XRD analysis, listed in Table 3. The discrepancy of calcium and aluminum not being detected in the EDS analysis may be attributed to their low content in the sample.

The elemental composition of the residue was further determined with ICP-OES, complementing the EDS findings. Fig. 3 shows the results for potassium and phosphorus, with error bars encompassing the deviation between the analysis methods. Concentrations after pyrolysis in N_2 at 800 °C (char) and 3 % O_2 at 1000 °C (ash) are depicted based on the concentration in the original fuel based on a dry solid basis. The disparity between the concentrations in the samples after pyrolysis or gasification and the original fuel is assumed to have been released into the gas phase during the corresponding experiment. Release of potassium during pyrolysis and gasification was negligible, with the measured concentration differences only being slightly larger than the analysis methods error. Conversely, phosphorus exhibits notable release to the gas phase during gasification.

Fig. 4 shows equilibrium phases from the calculations with the FactSage software, melt formation and the distribution of the elements in the solid, liquid, and gas phase. The solid phase primarily comprises various K-Mg-phosphates and K-Ca-phosphates, consistent with the phases identified via XRD. Melt formation, anticipated at temperatures above 675 °C, corresponds well with the observations from the SEM analysis. The melt, initially rich in potassium and phosphorus, becomes increasingly enriched in magnesium and calcium with increasing temperature. For the distribution of phosphorus and potassium between the condensed phase and the gas phase, the results from the equilibrium calculations and the experiments differ significantly. According to the equilibrium calculations, no potassium or phosphorus release is anticipated under the investigated conditions, while this was observed in the experiments.

The observed release of potassium and phosphorus to the gas phase may be explained by the carbothermic reduction of phosphates in the char. Recent studies by Lidman Olsson et al. provide evidence for such carbothermic reduction reactions during thermal conversion of plant-based biomass [26,27]. The overall reduction can be described by the simplified reactions (R1-R3) (Me = Ca or Mg).

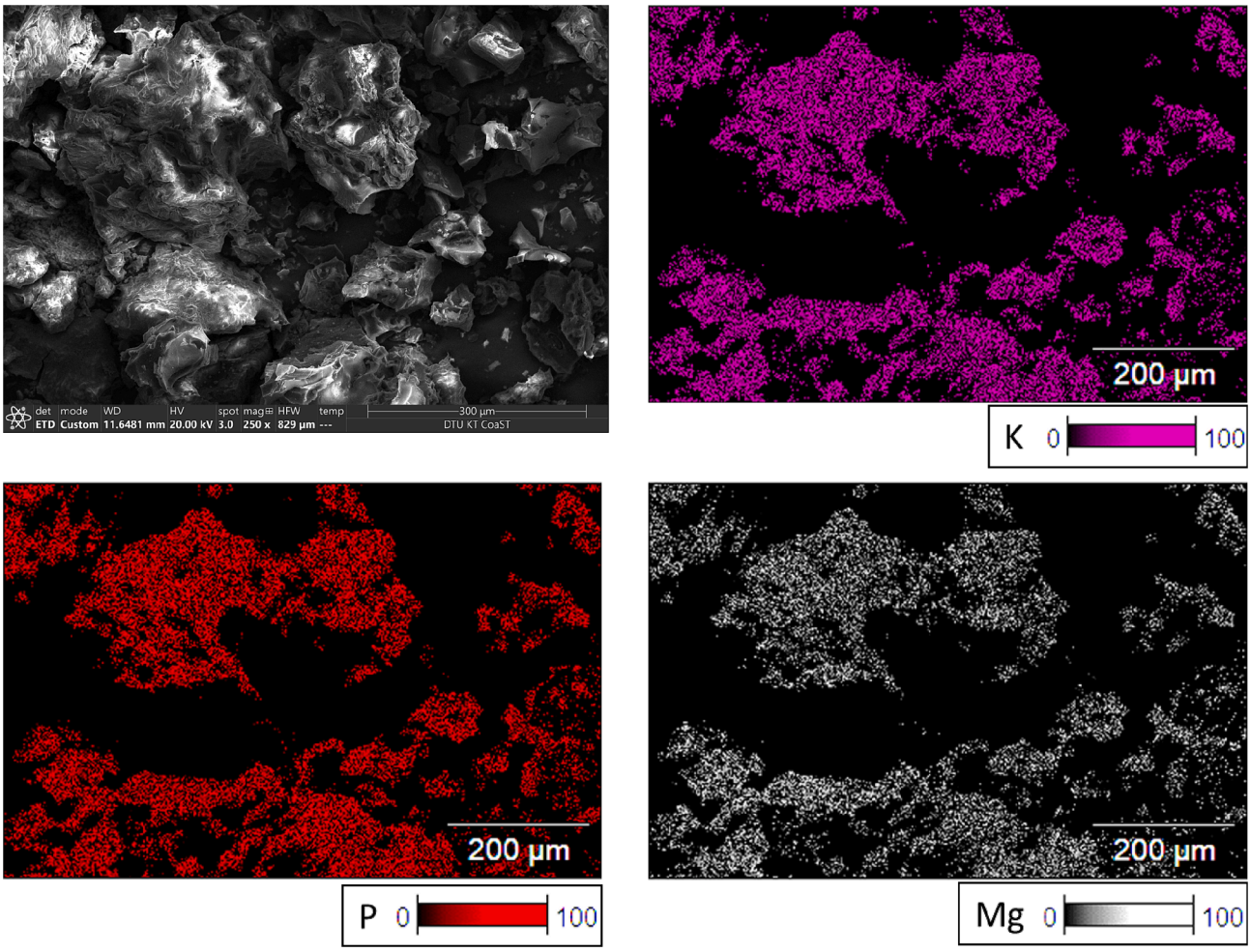

Fig. 2. SEM and EDS analysis of ash particles from gasification of WB at 1000°C in 3 % O_2 (rest N_2).

Table 3
Crystalline phases identified with XRD in wheat bran residue at 1000°C.

Phase	Chemical formula	ICDD pdf number
potassium magnesium phosphate	$KMgPO_4$	000–50-0146 000–50-0149 040–09-7824
potassium magnesium diphosphate	$K_2MgP_2O_7$	000–52-1084
potassium calcium diphosphate	$K_2CaP_2O_7$	000–50-1563
calcium diphosphate	$Ca_2P_2O_7$	040–09-6231
magnesium metaphosphate	$Mg(PO_3)_2$	000–11-0041
aluminium phosphate (berlinite)	$AlPO_4$	040–09-5763
silicon dioxide (tridymite)	SiO_2	010–77-8635
silicon dioxide (cristobalite)	SiO_2	040–08-7743

$$2\ Me(PO_3)_2(s) + 5C(s) \rightarrow Me_2P_2O_7(s) + 0.5P_4(g) + 5CO(g) \quad (R1)$$

$$3\ Me_2P_2O_7(s) + 5C(s) \rightarrow 2\ Me_3(PO_4)_2(s) + 0.5P_4(g) + 5CO(g) \quad (R2)$$

$$Me_3(PO_4)_2(s) + 5C(s) \rightarrow 3\ MeO(s) + 0.5P_4(g) + 5CO(g) \quad (R3)$$

Reactions involving alkali phosphates can be described similarly. Phosphorus exists in the gas phase as P_4 and may undergo further reactions. Carbothermic reactions are particularly relevant under low-oxygen conditions such as gasification, as carbon is more prone to react with oxygen than phosphates [26].

To verify whether carbothermic reduction reactions can explain the observations in the present study, an additional experiment was performed in which a filter was added to the outlet tube of the reactor in order to collect condensed species from the gas phase. Wheat bran char was utilized to reduce the amount of other interfering particles that are rapidly released during pyrolysis. The char was heated to 1100 °C in 100 % N_2 atmosphere. Upon removing the filter after the experiment, a distinct garlic smell was noted, typical for P_4O_6 (phosphorus trioxide), which can be formed when P_4 oxidizes [28]. This observation may confirm the release of phosphorus in its elemental form during

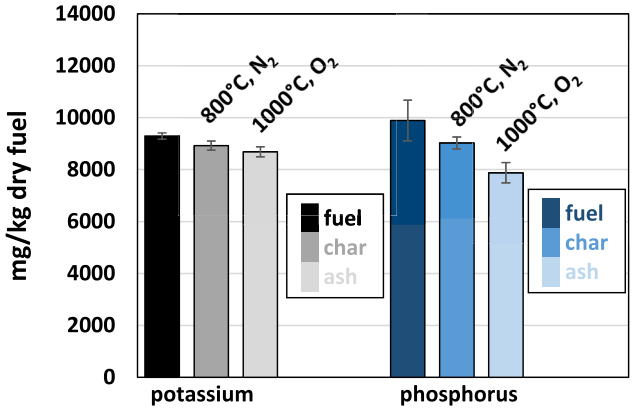

Fig. 3. Potassium and phosphorus of residuals after pyrolysis of wheat bran at 800 °C and gasification in 3 % O_2 at 1000°C.

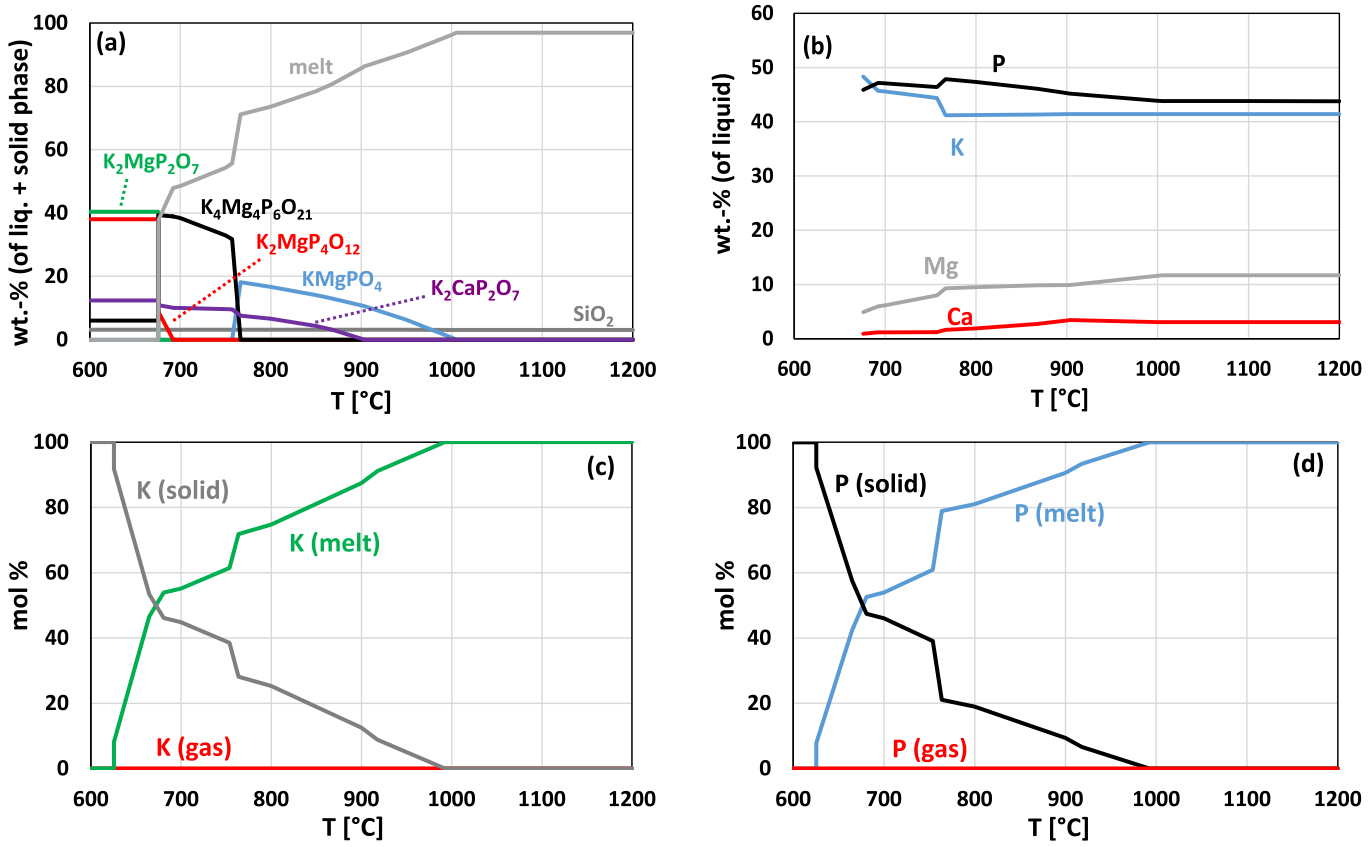

Fig. 4. Chemical equilibrium phases (a), composition of the liquid phase (excluding oxygen) and distribution of potassium and phosphorus in the solid, liquid and gas phases (c-d) under gasification conditions. Input: 10 g fuel (WB, elements based on fuel analysis) + 9.3 mol N_2 + 0.3 mol O_2.

gasification (compare R1-R3). In addition, phosphorus was identified by SEM-EDS on the filter paper, which is shown in Fig. 5. The SEM image revealed a fine layer containing phosphorus and potassium covering the filter, along with small crystals, possible potassium chloride (KCl). The presence of phosphorus and potassium in the thin layer suggests the likelihood of K-phosphate being the predominant species. From this test, it cannot be concluded weather the formation of K-phosphates occurred in the gas phase, or if it was formed from condensed species on the filter after the filter was removed and exposed to air. Nevertheless, the observations support the occurrence of carbothermic reduction reactions and enhance our understanding of the fate of phosphorus during the thermal conversion of phosphorus-rich biomasses.

The occurrence of carbothermic reduction reactions may also explain why chemical equilibrium calculations deviate from the experimental observations. Carbothermic reduction reactions can only occur if the phosphorus is able to react with carbon in the fuel, which is not possible if the carbon is consumed rapidly by oxygen. Additional chemical equilibrium calculations for oxygen-free conditions (see Fig. 1 in supplementary material) predicted a significant share of phosphorus in the gas phase for the investigated temperature range. The phosphorus release observed in the experiments may hence be explained by a low carbon conversion (e.g. caused by low mass transfer) which enabled the carbothermic reduction reactions. As the carbon conversion plays a significant role here, it can be concluded that chemical equilibrium calculations alone are not sufficient to predict the release of phosphorus to the gas phase, and kinetics should be considered as well.

3.2. Sunflower seed shells

The char yield for sunflower seed shells at 800 °C in 100 % N_2 was 23.9 ± 0.4 %. Subsequent gasification of the char samples in 3 % O_2 or 10 % CO_2 (rest N_2) to 900, 1000, or 1100 °C resulted in ash yields of 25.0 %, 19.0 % and 20.2 % in the cases with oxygen and 5.2 %, 4.29 % and 6.43 % in the cases with CO_2, respectively. Fig. 6 presents the SEM-EDS analysis of one of the residues after gasification in 1000 °C in 3 % O_2. Unlike wheat bran residues, sunflower seed shell residues exhibit diverse particle sizes and shapes, with varying chemical compositions. High phosphorus signals interface with calcium, suggesting the presence of hydroxyapatite. Hydroxyapatite, calcium oxide and magnesium oxide were identified via XRD analysis (see Table 4). Silica was found spread out evenly in the sample, but no crystalline phases containing silica were identified in the XRD analysis. The XRD spectra were similar for all residues from the experiments under the various gasification conditions. However, the chemical composition, i.e. the concentration of ash forming elements, differed.

Fig. 7 shows the potassium and phosphorus concentrations in the samples after pyrolysis and gasification experiments under the investigated conditions. The error bars account for the deviation between the SEM-EDS and ICP-OES analyses, with concentrations based on the original fuel content. Notably, a substantial amount of potassium was released to the gas phase in both oxygen- and CO_2-containing atmospheres. 75 % of the potassium was released at 1100 °C in the case with O_2 and 93 % in the case with CO_2 respectively. The amount of phosphorus remained constant for all samples within the measurement error, indicating that no significant phosphorus was released under the investigated conditions.

The predictions from the thermodynamic equilibrium calculations for sunflower seed shell residues are shown in Fig. 8. According to these, the only stable solid phase containing phosphorus is $KMgPO_4$, contradicting the findings from SEM-EDS and XRD analysis indicating hydroxyapatite presence. Localized higher concentrations of calcium and phosphorus in the fuel may explain this discrepancy, as increased

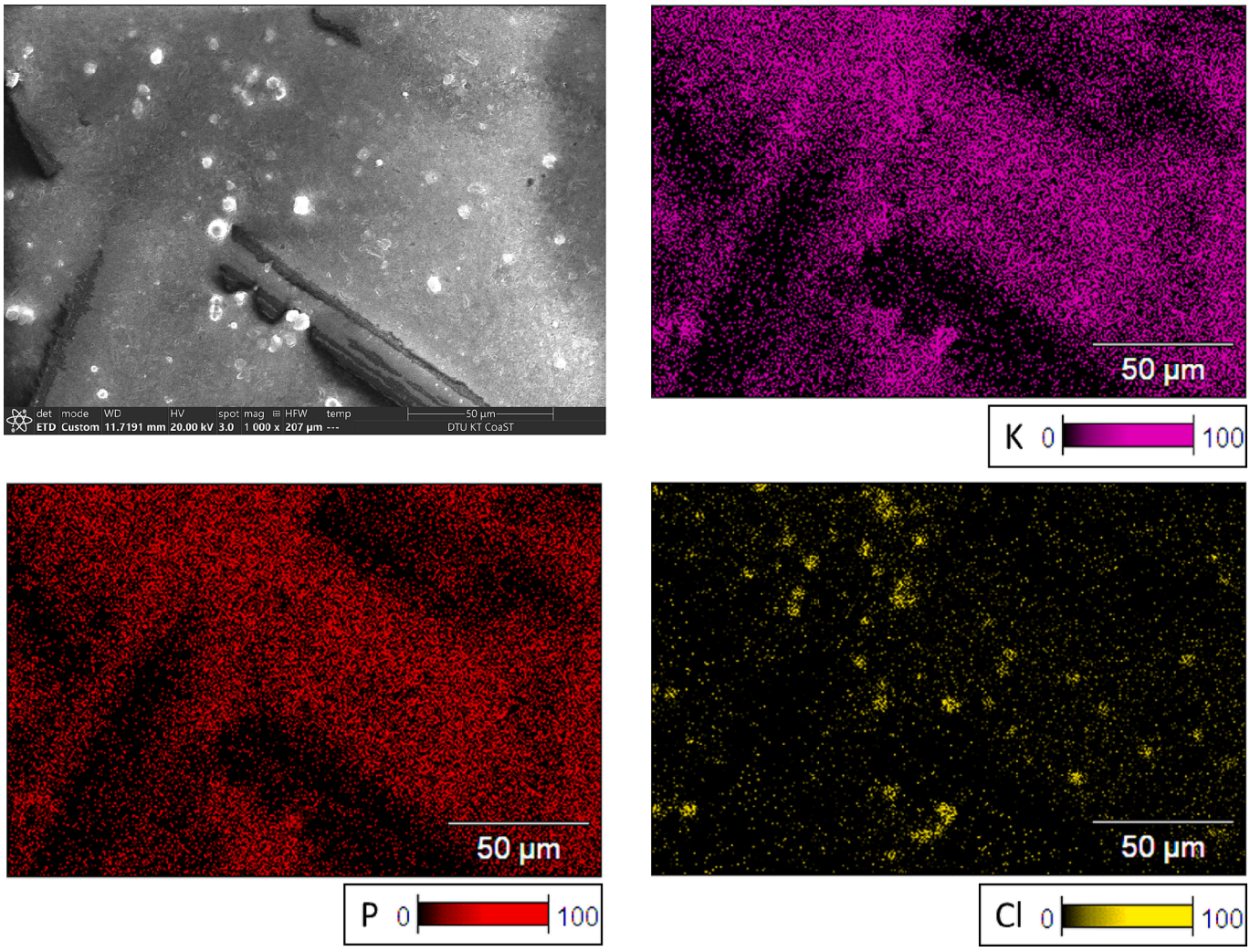

Fig. 5. SEM-EDS analysis of the filter added to the outlet tube after gasification of wheat bran char at 1100 °C in 100 % N_2.

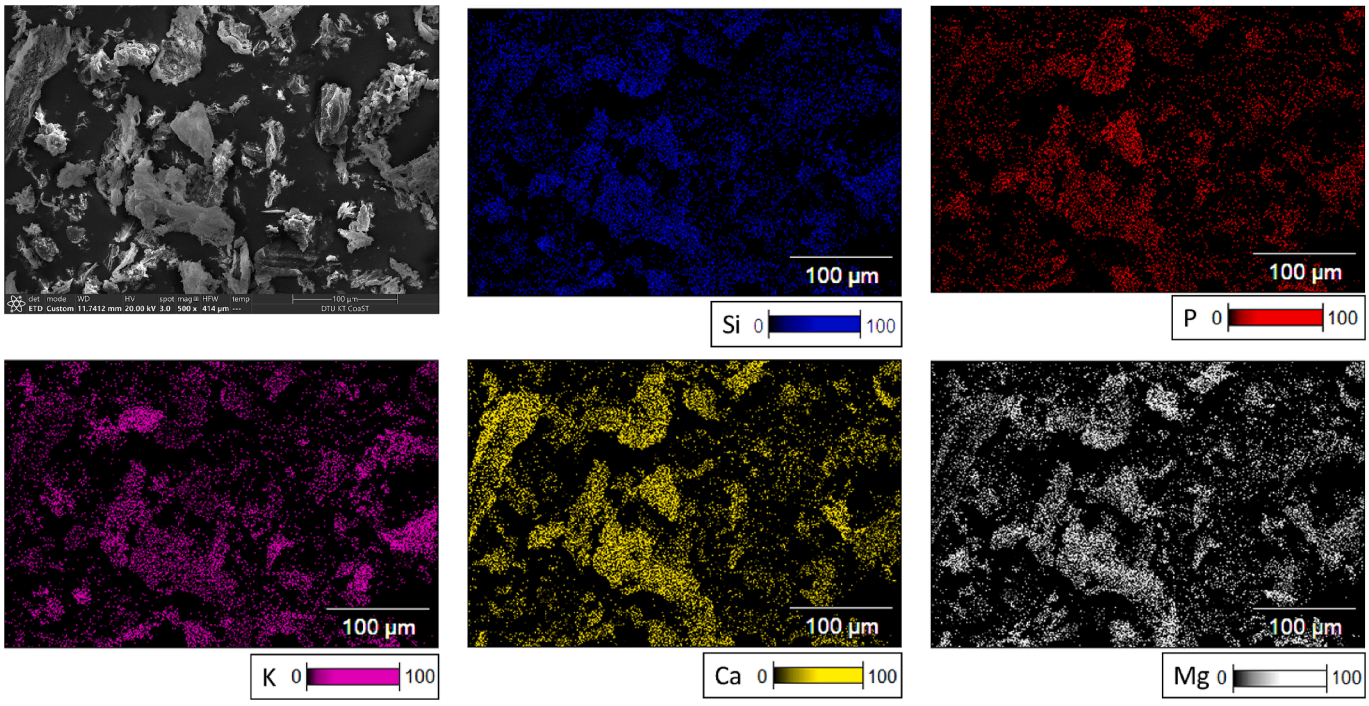

Fig. 6. SEM and EDS analysis of ash particles from gasification of sunflower seed shells at 1000°C in 3 % O_2 (rest N_2).

Table 4
Crystalline phases identified with XRD in sunflower seed shell residue at 1000°C.

Phase	Chemical formula	ICDD pdf number
calcium phosphate hydroxide (hydroxyapatite)	$Ca_{10}(PO_4)_6(OH)_2$	000–55-0592
calcium hydrogen phosphate hydroxide	$Ca_9H(PO_4)_6(OH)_2$	000–46-0905
magnesium oxide	MgO	040–16-6275
calcium oxide	CaO	010–77-9574

concentrations of those elements would favor hydroxyapatite also according to additional TE calculations. The presence of hydroxyapatite could account for the high observed potassium release, as more potassium is bound to the less stable silicates if no stable $KMgPO_4$ is formed. With increasing temperatures, more potassium is released from the silicates. The gasification atmosphere influenced the release of potassium. In the experiments with 10 % CO_2, more potassium was released as compared to the corresponding experiments with 3 % O_2. One possible explanation for the higher potassium release in the case with 10 % CO_2 could be the promoted formation of carbonates during the conversion, e.g. $CaCO_3$ and K_2CO_3, which would limit the formation of the more stable K-silicates. At the investigated temperatures, those carbonate decompose and K and KOH can be released from the K_2CO_3 to the gas phase. XRD analysis of the residues also revealed the presence of CaO, which would support the idea that less calcium is reacting with potassium than the equilibrium calculations predict. Hence, the equilibrium calculations are underestimating the potassium release. However, XRD analysis could not quantify the amount of CaO formed in the tests, so it cannot be said for sure this is the cause for higher potassium release in the tests with 10 % CO_2 as compared to the tests with 3 % O_2.

Additional chemical equilibrium calculations were performed for oxygen-free conditions (Fig. 2 supplementary material) to investigate whether the presence of oxygen may influence the phosphorus release, similar to wheat bran. In contrast to wheat bran, no phosphorus release is expected for sunflower seed shells for the investigated temperature range even under oxygen-free conditions.

4. Conclusions

This study investigated the fate of phosphorus and potassium during the gasification of agricultural biomass fuels. Residues from gasification of wheat bran and sunflower seed shells under various conditions were characterized and the release of phosphorus and potassium was quantified based on the analysis of the residues. The results were compared with thermodynamic predictions of the fate of the fuels in the experimental conditions.

- Wheat bran residues contained homogeneous particles of mainly K-Mg-phosphates. According to SEM images, the particles had melted during gasification at 1000 °C, as also suggested by thermodynamic equilibrium calculations.
- The residues from the gasification of sunflower seed shell consisted of heterogeneous particles with varying chemical compositions. SEM-EDS and XRD analysis revealed that some particles mainly contained hydroxyapatite, while others mainly contained K-Ca-silicates and K-Mg-silicates.
- During the gasification of sunflower seed shells, potassium was released whereas no phosphorus release was observed. The release of potassium was higher in a 10 % CO_2 atmosphere compared to a 3 % O_2 atmosphere. At 1100 °C, around 90 % of the potassium was released with 10 % CO_2 and 75 % with 3 % O_2 respectively. The higher potassium release with 10 % CO_2 is in agreement with the thermodynamic equilibrium calculations. However, both with 3 % O_2 and 10 % CO_2, the potassium release observed in the experiment was higher than suggested by the calculations.
- For wheat bran, thermodynamic equilibrium calculations differed significantly from the experimental observations. For wheat bran, all potassium and phosphorus was expected to remain in the residue under the investigated conditions based on the performed calculations. This, however, was not the case in the experiments. Around 20 % of the phosphorus from the fuel was released at 1000 °C. This observation may be explained by the occurrence of carbothermic reduction reactions, in which elemental phosphorus is released into the gas phase where it undergoes further reactions.

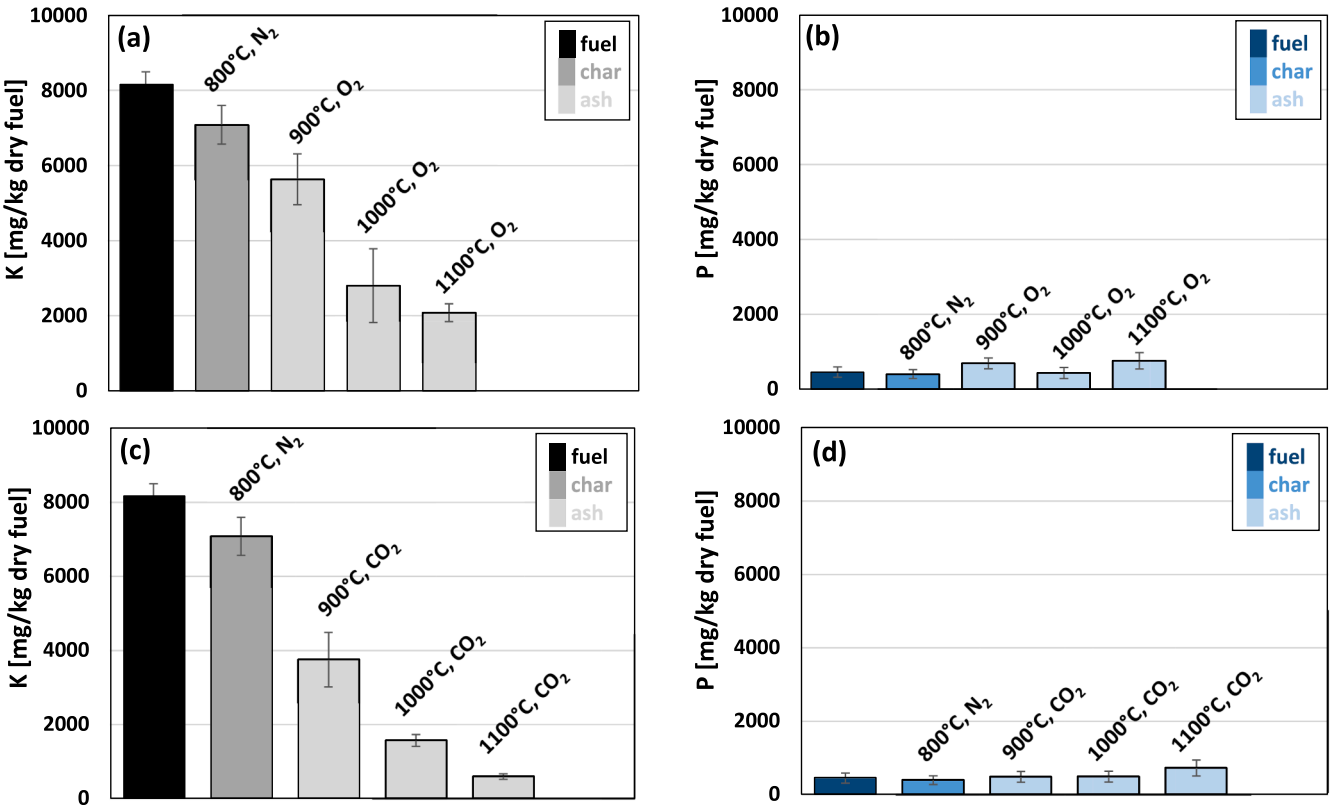

Fig. 7. Potassium and phosphorus of residuals after pyrolysis at 800 °C and gasification in 3 % O_2 (a-b) and 10 % CO_2 (d-e) at 900, 1000 and 1100°C.

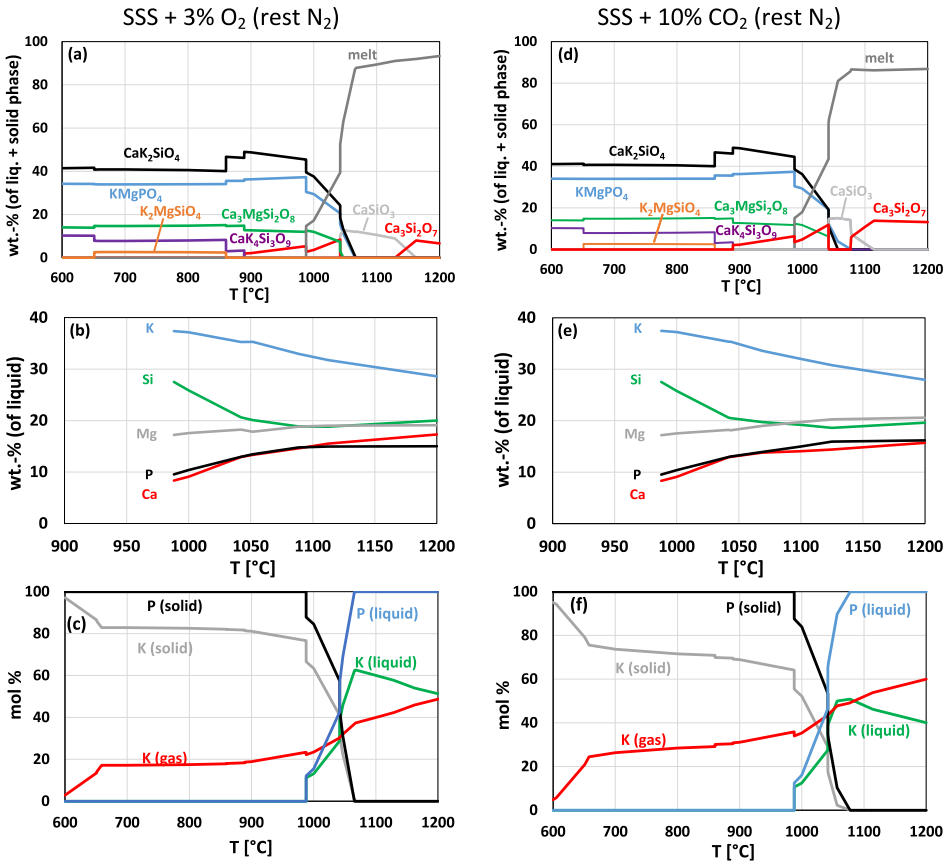

Fig. 8. Chemical equilibrium phases, composition of the liquid phase (excluding oxygen) and distribution of potassium and phosphorus in the solid, liquid and gas phase under gasification conditions. Input: 10 g fuel (SSS, elements based on fuel analysis) + 19.4 mol N_2 + 0.6 mol O_2 (a-c) or 18 mol N_2 + 2 mol CO_2 (d-f).

- As the kinetics of carbon consumption plays a key role for the occurrence of carbothermic reduction reactions, it is concluded that thermodynamic data alone is not enough to make predictions for the ash chemistry in thermal conversion processes using phosphorus rich biomass fuels. Further research needs to be conducted to improve predictions for the ash transformation chemistry of phosphorus-rich biomass fuels.

CRediT authorship contribution statement

Daniel Schmid: Writing – original draft, Investigation, Data curation. **Emil Lidman Olsson:** Writing – review & editing, Supervision. **Emil Vainio:** Writing – review & editing, Supervision. **Hao Wu:** Supervision, Funding acquisition. **Oskar Karlström:** Writing – review & editing, Funding acquisition. **Leena Hupa:** Writing – review & editing, Supervision, Funding acquisition.

Declaration of competing interest

The authors declare that they have no known competing financial interests or personal relationships that could have appeared to influence the work reported in this paper.

Acknowledgements

This project has received financial support from the Research Council of Finland financed projects High temperature chemistry of phosphorus – pathways to more effective recycling and utilization (341405), Chemical challenges in gasification of biomass and waste (355914 and 321598), and Nordic Energy Research project NEST – Nordic Network in Solid Fuels towards Future Energy Systems (120626).

Appendix A. Supplementary material

Supplementary data to this article can be found online at https://doi.org/10.1016/j.fuel.2024.133950.

Data availability

Data will be made available on request.

References

[1] Tezer Ö, Karabağ N, Öngen A, Çolpan CÖ, Ayol A. Biomass gasification for sustainable energy production: a review. Int J Hydrogen Energy 2022;47:15419–33.
[2] C. Higman, Gasification, In: Combustion Engineering Issues for Solid Fuel Systems, 2008: pp. 423–468.
[3] He Z, Lane DJ, Saw WL, Van Eyk PJ, Nathan GJ, Ashman PJ. Ash-bed material interaction during the combustion and steam gasification of australian agricultural residues. Energy Fuel 2018;32:4278–90.
[4] Grimm A, Skoglund N, Boström D, Öhman M. Bed agglomeration characteristics in fluidized quartz bed combustion of phosphorus-rich biomass fuels. Energy Fuel 2011;25:937–47.
[5] Abioye KJ, Harun NY, Sufian S, Yusuf M, Jagaba AH, Ekeoma BC, et al. A review of biomass ash related problems: mechanism, solution, and outlook. J Energy Inst 2024;112:101490.
[6] Niemi J, Engblom M, Laurén T, Yrjas P, Lehmusto J, Hupa M, et al. Superheater deposits and corrosion in temperature gradient – laboratory studies into effects of flue gas composition, initial deposit structure, and exposure time. Energy 2021;228:120494.
[7] Wei J, Wang M, Xu D, Shi L, Li B, Bai Y, et al. Migration and transformation of alkali/alkaline earth metal species during biomass and coal co-gasification: a review. Fuel Process Technol 2022;235:107376.
[8] Woolcock PJ, Brown RC. A review of cleaning technologies for biomass-derived syngas. Biomass Bioenergy 2013;52:54–84.
[9] Lisi L, Cimino S. Poisoning of scr catalysts by alkali and alkaline earth metals. Catalysts 2020;10:1475.

[10] Szymaszek A, Samojeden B, Motak M. The deactivation of industrial SCR catalysts—a short review. Energies (Basel) 2020;13:3870.
[11] Falk J, Skoglund N, Grimm A, Öhman M. Systematic evaluation of the fate of phosphorus in fluidized bed combustion of biomass and sewage sludge. Energy Fuel 2020;34:3984–95.
[12] Hannl TK, Häggström G, Hedayati A, Skoglund N, Kuba M, Öhman M. Ash transformation during single-pellet gasification of sewage sludge and mixtures with agricultural residues with a focus on phosphorus. Fuel Process Technol 2022;227:107102.
[13] Deng L, Huang X, Tie Y, Jiang J, Zhang K, Ma S, et al. Experimental study on transformation of alkali and alkaline earth metals during biomass gasification. J Energy Inst 2022;103:117–27.
[14] Ge Y, Ding S, Kong X, Kantarelis E, Engvall K, Pettersson JBC. Real-time monitoring of alkali release during CO_2 gasification of different types of biochar. Fuel 2022;327:125102.
[15] Stankowski S, Chajduk E, Osińska B, Gibczyńska M. Biomass ash as a potential raw material for the production of mineral fertilisers. Agron Res 2021;19:1999–2012.
[16] Zhu F, Cakmak EK, Ceteciogluz Z. Phosphorus recovery for circular economy: application potential of feasible resources and engineering processes in Europe. Chem Eng J 2023;454:140153.
[17] Vassilev SV, Vassileva CG, Bai J. Content, modes of occurrence, and significance of phosphorous in biomass and biomass ash. J Energy Inst 2023;108.
[18] Odzijewicz JI, Wołejko E, Wydro U, Wasil M, Jabłońska-Trypuć A. Utilization of ashes from biomass combustion. Energies (Basel) 2022;15:9653.
[19] Dizaji HB, Zeng T, Lenz V, Enke D. Valorization of residues from energy conversion of biomass for advanced and sustainable material applications. Sustain (Switzerland) 2022;14:4939.
[20] Lidman Olsson EO, Glarborg P, Leion H, Dam-Johansen K, Wu H. Release of P from pyrolysis, combustion, and gasification of biomass - a model compound study. Energy Fuel 2021;35:15817–30.
[21] Hedayati A, Falk J, Borén E, Lindgren R, Skoglund N, Boman C, et al. Ash transformation during fixed-bed combustion of agricultural biomass with a focus on potassium and phosphorus. Energy Fuel 2022;36:3640–53.
[22] Silva FC, Cruz NC, Tarelho LAC, Rodrigues SM. Use of biomass ash-based materials as soil fertilisers: critical review of the existing regulatory framework. J Clean Prod 2019;214:112–24.
[23] Garcia-Maraver A, Mata-Sanchez J, Carpio M, Perez-Jimenez JA. Critical review of predictive coefficients for biomass ash deposition tendency. J Energy Inst 2017;90:214–28.
[24] Atallah E, Defoort F, Pisch A, Dupont C. Thermodynamic equilibrium approach to predict the inorganic interactions of ash from biomass and their mixtures: a critical assessment. Fuel Process Technol 2022;235:107369.
[25] Bale CW, Bélisle E, Chartrand P, Decterov SA, Eriksson G, Gheribi AE, et al. Reprint of: FactSage thermochemical software and databases, 2010–2016. Calphad 2016;55:1–19.
[26] Lidman Olsson EO, Schmid D, Karlström O, Enemark-Rasmussen K, Leion H, Li S, et al. Release of phosphorus from thermal conversion of phosphorus-rich biomass chars – evidence for carbothermic reduction of phosphates. Fuel 2023;341:127706.
[27] Lidman Olsson EO, Glarborg P, Leion H, Dam-Johansen K, Wu H. An exploratory study of phosphorus release from biomass by carbothermic reduction reactions. Proc Combust Inst 2023;39:3271–81.
[28] Sidell FR, Takafuji ET, Franz DR. Med Asp Chem Biol Warfare 1997.